Multichannel Blind Iterative Image Restoration

Filip Šroubek and Jan Flusser, *Senior Member, IEEE*

***Abstract*— Blind image deconvolution is required in many applications of microscopy imaging, remote sensing, and astronomical imaging. Unfortunately in a single-channel framework, serious conceptual and numerical problems are often encountered. Very recently, an eigenvector-based method (EVAM) was proposed for a multichannel framework which determines perfectly convolution masks in a noise-free environment if channel disparity, called co-primeness, is satisfied. We propose a novel iterative algorithm based on recent anisotropic denoising techniques of total variation and a Mumford-Shah functional with the EVAM restoration condition included. A linearization scheme of half-quadratic regularization together with a cell-centered finite difference discretization scheme is used in the algorithm and provides a unified approach to the solution of total variation or Mumford-Shah. The algorithm performs well even on very noisy images and does not require an exact estimation of mask orders. We demonstrate capabilities of the algorithm on synthetic data. Finally, the algorithm is applied to defocused images taken with a digital camera and to data from astronomical ground-based observations of the Sun.**

***Index Terms*— multichannel blind deconvolution, total variation, Mumford-Shah functional, half-quadratic regularization, subspace methods, conjugate gradient**

I. Introduction

BLIND restoration of an image acquired in an erroneous measuring process is often encountered in image processing but a satisfying solution to this problem has not been yet discovered. The amount of a priori information about degradation, i.e., the size or shape of blurs, and the noise level, determines how mathematically ill-posed the problem is. Even nonblind restoration, when blurs are available, is in general an ill-posed problem because of zeros in the frequency domain of the blurs. The single-channel (SC) blind and nonblind deconvolution in 2-D have been extensively studied and many techniques have been proposed for their solution [1], [2]. They usually involve some regularization which assures various statistical properties of the image or constrains the estimated image and/or restoration filter according to some assumptions. This regularization is required to guarantee a unique solution and stability against noise and some model discrepancies. SC restoration methods that have evolved from denoising applications form a very successful branch. Anisotropic denoising techniques play a prominent role due to their inherent ability to preserve edges in images. Total variation (TV) has proved to be a good candidate for edge-preserving denoising [3]. The TV solution is associated with highly nonlinear Euler-Lagrange equations but several linearization schemes were proposed to deal with this nonlinearity: the fixed point iteration scheme [4], [5], the primal-dual method [6] or a more general half-quadratic regularization scheme proposed in [7]. Recently, a more sophisticated approach, which minimizes the Mumford-Shah energy function [8], was successfully applied to image denoising and segmentation [9]. A trivial extension into the nonblind deconvolution problem exists for all these iterative denoising techniques.

A breakthrough in understanding of blind deconvolution was the method of zero sheets proposed by Lane and Bates [10]. They have shown that the SC blind deconvolution is possible in a noise-free case. Their arguments rest on the analytical properties of the z-transform in 2-D and on the fact that 2-D polynomials are not generally factorizable. Although conceptually the zero sheets are correct, they have little practical application since the algorithm is highly sensitive to noise and prone to numerical inaccuracy for large image sizes. A famous pioneering work in blind deconvolution has been done by Ayers and Dainty [11] (Interesting are also enhancements proposed in [12], [13], [14]). Their iterative method based on Wiener-like filters with the possibility to include all sorts of constraints is robust to noise but lacks any reliability, since the problem of blind deconvolution is ill-posed with respect to both the image and the blur. If the images are smooth and homogeneous, an autoregressive model can be used to describe the measuring process. The autoregressive model simplifies the blind problem by reducing the number of unknowns and several techniques were proposed for finding its solution [15], [16], [17]. Very promising results have been achieved with a nonnegativity and support constraints recursive inverse filtering (NAS-RIF) algorithm proposed by Kundur and Hatzinakos [2] and extensions in [18], [19]. These methods, however, work on images that contain objects of finite support and have a uniform background. The area of the object support must be determined in advance. A bold attempt [20] has been made to use the TV-based reconstruction for the blind SC problems but with dubious results as the problem is ill-posed with respect to both the image and the blur. The alternating minimization algorithm has been proposed for this purpose and Chan et al. [21] have verified its convergence in case of the L_2 norm of the image gradient, but not in case of the TV functional.

The knowledge of the degradation process does not have to be the only source of useful a priori information. Multiple acquisition that generates several differently blurred versions of one scene may provided the information. Examples of such multichannel (MC) measuring processes are not rare and include remote sensing and astronomy, where the same scene is observed at different time instants through a time-varying

Financial support of this research was provided by the Grant Agency of the Czech Republic under the project No. 102/00/1711.

Filip Šroubek and Jan Flusser are with the Institute of Information Theory and Automation, Academy of Sciences of the Czech Republic, Pod vodárenskou věží 4, 182 08 Prague 8, Czech Republic, E-mail: {sroubekf,flusser}@utia.cas.cz

inhomogeneous medium such as the atmosphere; electron microscopy, where images of the same sample are acquired at different focusing lengths; or broadband imaging through a physically stable medium but which has a different transfer function at different frequencies. The MC acquisition refers in general to two input/output models that differ fundamentally, and from the mathematical point of view, should be distinguished: the single-input multiple-output (SIMO) model and the multiple-input multiple-output (MIMO) model. The SIMO model is typical for one-sensor imaging under varying environment conditions, where individual channels represent the conditions at time of acquisition. The MIMO model refers to multi-sensor or broadband imaging, where the channels represent, for example, different frequency bands or resolution levels. Color images are the special case of the MIMO model. An advantage of MIMO is the ability to model cross-channel degradations which occur in the form of channel crosstalks, leakages in detectors, and spectral blurs. Many techniques for solving the MIMO problem were proposed and could be found in [22], [23], [24], [25]. In the sequel, we confine ourselves to the SIMO model exclusively and any reference to the term MC denotes the SIMO model.

Nonblind MC deconvolution is potentially free of the problems arising from the zeros of blurs. The lack of information from one blur in one frequency is supplemented by the information at the same frequency from others. It follows that the blind deconvolution problem is greatly simplified by the availability of several different channels. Moreover, it is possible to estimate the blur functions directly by a simple one-step procedure and reduce the blind problem to the nonblind one if certain conditions are met. Harikumar and Bresler proposed in [26], [27] a very elegant one-step subspace procedure (EVAM) which accomplishes perfect blind restoration in a noise-free environment by finding a minimum eigenvector of a MC condition matrix. One disadvantage of EVAM is its vulnerability to noise. Even for a moderate noise level the restoration may break down. Pillai et al. [28] have proposed another intrinsically MC method based on the greatest common divisor which is, unfortunately, even less numerically stable. A different, also intrinsically MC, approach proposed in [29] first constructs inverse FIR filters and then estimates the original image by passing the degraded images through the inverse filters. Noise amplification also occurs here but can be attenuated to a certain extent by increasing the inverse filter order, which comes at the expense of deblurring.

The above reasoning implies that the combination of the anisotropic denoising technique with the subspace procedure could provide both the numerical stability and the necessary robustness to noise. In the paper, we thus propose an MC alternating minimization algorithm (MC-AM) which incorporates the EVAM condition matrix into the anisotropic denoising technique as an extra regularization term. We derive the algorithm for two different denoising approaches: total variation and Mumford-Shah functional; and discuss in detail linearization and discretization schemes which lead in both cases to simple equations that differ only in the construction of one particular matrix.

The rest of this paper is organized as follows. Used notation and few numerical considerations are presented in Section II. Section III provides mathematical preliminaries for the development of the algorithm, which is then described in Section IV. Results of three experiments conducted on artificial and real data, and comparisons with the simple EVAM method are given in Section V.

II. Notation and Definitions

Throughout, Ω will denote a rectangle in $\mathbb{R}^2$ (although lower or higher dimensions may be also considered) which is the definition domain of image intensity functions. All the image intensity functions will be regarded as a bounded gray-level functions of the form $u : \Omega \to [0,1]$. $\mathbf{x} = (x,y)$ denotes location in Ω, $|\mathbf{x}| = \sqrt{x^2+y^2}$ denotes Euclidian norm, and $\|\cdot\|$ denotes the norm in $L_2(\Omega)$. $|E|$ stands for the Lebesgue measure of $E \subseteq \mathbb{R}^2$ which could be considered to be equal to the area of E.

To be able to implement the proposed algorithm a proper discretization is necessary. We will follow the CCFD (cell-centered finite difference) discretization scheme [5]. A square lattice is constructed on top of Ω with a constant step h. Let m and n denote the minimum number of cells in the y and x directions, respectively, that covers the total area of Ω. A cell $c_{ij} \subseteq \Omega$ is defined as

$$c_{ij} = \{(x,y) : (i-1/2)h \le y \le (i+1/2)h, \\ (j-1/2)h \le x \le (j+1/2)h\}$$

with area $|c_{ij}| = h^2$. The cell centers are given by (x_j, y_i) and indexed (i,j), where

$$x_j = (j-1/2)h, \quad j = 1,\dots,n\,, \\ y_i = (i-1/2)h, \quad i = 1,\dots,m\,.$$

The cell middle edge points are given by $(x_{j\pm1/2}, y_{i\pm1/2})$ and indexed $(i \pm 1/2, j \pm 1/2)$, where

$$x_{j\pm1/2} = x_j \pm (h/2)\,, \\ y_{i\pm1/2} = y_i \pm (h/2)\,.$$

Function $u(\mathbf{x})$ is then approximated by a piecewise constant function $U(\mathbf{x})$ which has a constant value u_{ij} inside the cell c_{ij}. u_{ij} is often calculated as the mean of $u(\mathbf{x})$ over the cell c_{ij} or simply the value of u at the cell center (i,j). The set of u_{ij} values fully defines the piecewise constant function $U(\mathbf{x})$ which can be thus regarded as a discrete matrix $\mathbf{U} = \{u_{ij}\}$ of size (m,n). The 2-D discrete z-transform of $\mathbf{U}$ is defined as $\tilde{U}(z_1,z_2) = \sum_{i=1}^{m}\sum_{j=1}^{n} u_{ij} z_1^{-i} z_2^{-j}$, where $z_1, z_2 \in \mathbb{C}$. Finally, $\mathbf{u} \in \mathbb{R}^{mn}$ denotes the discrete vector representation of the image function $u(\mathbf{x})$ and is obtained by lexicographically ordering u_{ij} with respect to the index pair (i,j). Any linear operator $K(\cdot)$ and operation $K(u)(\mathbf{x})$ can be thus approximated by a discrete matrix $\mathbf{K}$ and matrix-vector multiplication $\mathbf{Ku}$, respectively.

In the sequel, the symbol $*$ will denote 2D convolution. Using the vector-matrix notation, the convolution $h * u$ is approximated by $\mathbf{C_H u}$, where $\mathbf{C_H}$ is a block Toeplitz matrix with Toeplitz blocks. If spatial periodicity of functions is

assumed, standard convolution could be replaced with circular convolution, which is represented in the discrete space by a block circular matrix with circular blocks. The Fourier transform (FT) simplifies circular matrices to diagonal matrices, and clearly, this is a very useful property which justifies the periodic assumption.

Before we proceed on, it is crucial to investigate the discretization of flux variables. Let us consider the amount v of image gradient ∇u flowing in the direction $\mathbf{n}$, $v(\mathbf{x},\mathbf{n}) = \left\langle \left(\frac{\partial u}{\partial x}(\mathbf{x}), \frac{\partial u}{\partial y}(\mathbf{x})\right), \mathbf{n}\right\rangle$, where $\langle\cdot,\cdot\rangle$ denotes the scalar product. The discretization of $\nabla u(\mathbf{x})$ follows the CCFD scheme. However, the normal vector $\mathbf{n}$ has a finite number of directions in the discrete space. The most simplified approximation (four–connectivity) defines only two main directions $(1,0),(0,1)$ and the corresponding discrete flux v is defined at the cell middle edge points as $v((x_j,y_i),(0,1)) \approx v_{i+1/2,j} = |u_{i+1,j} - u_{i,j}|/h$, $v((x_j,y_i),(1,0)) \approx v_{i,j+1/2} = |u_{i,j+1} - u_{i,j}|/h$. A more accurate approximation (eight–connectivity) would include, apart from the two main directions, additional two diagonal directions $(1,1),(-1,1)$ that define flux values at the cell corners as $v_{i+1/2,i+1/2} = |u_{i+1,j+1} - u_{i,j}|/\sqrt{2h^2}$ and $v_{i+1/2,j-1/2} = |u_{i+1,j-1} - u_{i,j}|/\sqrt{2h^2}$.

III. Mathematical preliminaries

Consider the MC (SIMO) model that consists of P measurements of an original image u. The relation between recorded images z_p and the original image u is described by the equation

$$z_p(\mathbf{x}) = (h_p * u)(\mathbf{x}) + n_p(\mathbf{x}), \quad \mathbf{x}\in\Omega, \quad p = 1,\dots,P\,, \tag{1}$$

where h_p is the point spread function (PSF) of the p-th channel blur, and n_p is signal independent noise. Note, that the only known variables are z_p. As the blind deconvolution problem is ill-posed with respect to both u and h_p, a constrained minimization technique is required to find the solution of (1). Constraints considered here are very common in real acquisition processes and thus widely accepted. Assuming white noise (with diagonal correlation matrix) of zero mean and constant variance σ^2, and PSF's preserving energy, the imposed constraints take the following form,

$$\int_\Omega (h_p * u - z_p)^2 \,\mathrm{d}\mathbf{x} = |\Omega|\sigma^2, \quad p = 1,\dots,P\,, \tag{2}$$

$$\int_\Omega (z_p - u)\,\mathrm{d}\mathbf{x} = 0, \quad p = 1,\dots,P\,. \tag{3}$$

Let $Q(u)$ and $R(h_p)$ denote some regularization functionals of the estimated original image u and PSF's h_p, respectively. The constrained minimization problem is formulated as $\min_{u,h_p} Q(u) + R(h_p)$ subject to (1), (2) and (3). The unconstrained optimization problem, obtained by means of the Lagrange multipliers, is to find u and h_p which minimize the functional

$$E(u,h_1,\dots,h_P) = \frac{1}{2}\sum_{p=1}^{P} \|h_p * u - z_p\|^2 + \lambda Q(u) + \gamma R(h_1,\dots,h_P)\,, \tag{4}$$

where λ and γ are positive parameters which penalize the regularity of the solutions u and h_p. Constraint (3) is automatically satisfied under certain conditions as it will be clear later. For now, the crucial question is how the functionals Q and R should look like. We proceed the discussion first with possible choices for $Q(u)$ and then for $R(h_p)$.

A. Regularization term $Q(u)$

Regularization of (1) with respect to the image function can adopt various forms. The classical approach of Tichonov chooses $Q(u) = \int_\Omega |\nabla u|^2$. The corresponding non-blind minimization problem can be easily solved using FT and is equivalent to Wiener filtering. However, this advantage is only computational, because the obtained results are poor. The functional assumes u is smooth and any discontinuities in u create ringing artifacts. In the space of bounded variation functions where TV serves as seminorm, it is possible to define correctly image gradient together with discontinuities. Therefore, the TV convex functional was proposed by Rudin et al. [3] as the appropriate regularization functional,

$$Q_{TV}(u) \equiv \int_\Omega |\nabla u|\,. \tag{5}$$

The associated Euler-Lagrange equations of (4) with respect to u are

$$\begin{aligned} \frac{\partial E}{\partial u} &= \sum_p \mathcal{C}^*_{h_p}(\mathcal{C}_{h_p}(u) - z_p) - \lambda\nabla\cdot\left(\frac{\nabla u}{|\nabla u|}\right) \\ \frac{\partial u}{\partial n} &= 0 \quad \text{on } \partial\Omega\,, \end{aligned} \tag{6}$$

where $\mathcal{C}_{h_p}(\cdot) \equiv (h_p * \cdot)$ and $\mathcal{C}^*_{h_p}(\cdot)$ denotes the adjoint operator, which is in our case $\mathcal{C}^*_{h_p}(\cdot) = (h_p(-\mathbf{x}) * \cdot)$. In the second equation, $\frac{\partial u}{\partial n}$ is the directional derivative in the direction of the vector normal to the domain boundary $\partial\Omega$. Let us assume that the PSF's h_p are known. It was mentioned in the introduction that this equation is highly nonlinear, and moreover, not defined for $|\nabla u| = 0$. Several techniques were proposed to solve (6). We follow the linearization scheme described in [30] which is similar to the half-quadratic regularization scheme of D. Geman [7] and which could be easily applied to more complex functionals of the Mumford-Shah kind. The scheme introduces "an auxiliary variable" which transfers the problem to a more feasible one. Note that for every $x\in\mathbb{R}$, $x\neq 0$, $|x| = \min_{v>0}\left(\frac{v}{2}x^2 + \frac{1}{2v}\right)$ and the minimum is reached for $v = 1/|x|$. For numerical reasons, it is necessary to restrict v on a closed set $K_\epsilon = \{v : \epsilon \le v \le 1/\epsilon\}$. Substituting the above relation into (5), we obtain a functional of two variables

$$Q_\epsilon(u,v) = \frac{1}{2}\int_\Omega \left(v|\nabla u|^2 + \frac{1}{v}\right)\,, \tag{7}$$

and the algorithm consists of alternating minimizations of $F_\epsilon(u,v) = \lambda Q_\epsilon(u,v) + \frac{1}{2}\sum_p \|\mathcal{C}_{h_p}(u) - z_p\|^2$ over u and v. For any starting values u^0 and v^0, the steps $n\ge 1$ are

$$\begin{aligned} u^n &= \arg\min_u F_\epsilon(u, v^{n-1}) \quad \text{and} \\ v^n &= \arg\min_{v\in K_\epsilon} F_\epsilon(u^n, v) = \min(\max(\epsilon, 1/|\nabla u^n|), 1/\epsilon)\,. \end{aligned} \tag{8}$$

The minimization over v is trivial and the minimization over u is also simple, since $F_\epsilon(u,v)$ is convex and quadratic with respect to u. Convergence of the algorithm to the minimizer u_ϵ of F_ϵ is proved in [30]. Moreover, it is proved that F_ϵ converges to the original functional $F(u,v) = \lambda Q_{TV}(u) + \frac{1}{2}\sum_p \|\mathcal{C}_{h_p}(u) - z_p\|^2$ as $\epsilon \to 0$ but in a weak sense. This weaker notion of convergence, called Γ–*convergence*, was introduced for studying the limit of variational problems. It states that if the sequence (or a subsequence) of minimizers u_ϵ convereges to some u then u is a minimizer for F and $F_\epsilon(u_\epsilon) \to F(u)$. For each case, v is given by the second equation in (8).

In the late 80s, Mumford and Shah [8] have proposed a very complex energy function designed for image segmentation which depends on the image function u and the size of discontinuity set. In order to study the energy function, a weak formulation which depends solely on u was introduced. The regularization term of the weak Mumford-Shah energy is then

$$Q_{MS}(u) \equiv \int_\Omega |\nabla u|^2 \, + \, \mu \mathcal{H}^1(S_u)\,, \tag{9}$$

where $\mathcal{H}^1$ denotes the 1-D Hausdorff measure and $S_u \in \Omega$ is the 1-D set on which u is not continuous. The gradient ∇u is defined everywhere outside S_u. What follows is derived from Chambolle [9]. Let $U(\mathbf{x})$ denotes the piecewise constant approximation of $u(\mathbf{x})$ as described in Sec. II. Let the set of cell centers be $C_\Omega = \{(x_j, y_i) : i = 1,\ldots,m;\ j = 1,\ldots,n\} \subset \Omega$. Consider a functional

$$Q_h(U) = h^2 \sum_{\mathbf{x}\in C_\Omega} \sum_{\substack{\xi\in\mathbb{Z}^2 \\ \mathbf{x}+h\xi\in\Omega}} \frac{\mu}{h} f\left(\frac{(U(\mathbf{x}) - U(\mathbf{x}+h\xi))^2}{\mu h}\right)\phi(\xi), \tag{10}$$

where $\phi : \mathbb{Z}^2 \to \mathbb{R}^+$ is even, satisfies $\phi(0) = 0$, and $\phi(e_i) > 0$ for any $i = 1, 2$ where $\{e_1, e_2\}$ is the basis of $\mathbb{R}^2$; $f : \mathbb{R}^+ \to \mathbb{R}^+$ is a non-decreasing bounded function that satisfies $f(0) = 0$, $f(+\infty) = 1$, and $f'(0) = 1$. A good candidate for f is, for example, $f(t) = \frac{2}{\pi}\arctan\frac{\pi t}{2}$. According to [9], Q_h Γ–converges to a close approximation of the weak Mumford-Shah energy (9). The proximity is chiefly influenced by the course of function ϕ. Due to the high non-convexity in (10), the numerical computation of an exact minimizer is not guaranteed. If, in addition to the previous assumptions about f, we assume that f is concave and differentiable, we may write

$$f(x) = \min_{0\le v\le 1} xv + \psi(v)\,, \tag{11}$$

and the minimum is reached for $v = f'(x)$. We do not have to be concerned about the shape of $\psi(v)$, since ψ will vanish in the minimization procedure. We may therefore combine (11) with (10) and obtain a functional of two variables

$$Q_h(U,V) = h^2 \sum_{\mathbf{x}\in C_\Omega} \sum_{\substack{\xi\in\mathbb{Z}^2 \\ \mathbf{x}+h\xi\in\Omega}} \left[\mu\frac{\psi(V(\mathbf{x},h\xi))}{h} + V(\mathbf{x},h\xi)\left|\frac{U(\mathbf{x}) - U(\mathbf{x}+h\xi)}{h}\right|^2\right]\phi(\xi)\,, \tag{12}$$

where $V : C_\Omega \times h\mathbb{Z}^2 \to [0,1]$. The minimization algorithm is similar to (8) and consists of alternating minimizations of $F_h(U,V) = \lambda Q_h(U,V) + \frac{1}{2}\sum_p \|\mathcal{C}_{H_p}(U) - Z_p\|^2$ with respect to U and V. The iteration steps are as follows

$$\begin{aligned} U^n &= \arg\min_U F_h(U, V^{n-1}) \quad \text{and} \\ V^n(\mathbf{x}, h\xi) &= f'\left(\frac{(U(\mathbf{x}) - U(\mathbf{x}+h\xi))^2}{\mu h}\right)\,. \end{aligned} \tag{13}$$

The minimization over V is straightforward and the minimization over U is a simple problem, since $F_h(U,V)$ is convex and quadratic with respect to U.

B. Regularization term $R(h_p)$

We show regularization of (1) with respect to the blurs h_p. The discrete noise-free representation of equation (1) that conforms to the discretization scheme in Sec. II is given as follows:

$$\mathbf{Z}_p = \mathbf{H}_p * \mathbf{U}, \quad p = 1,\ldots,P\,, \tag{14}$$

where matrices $\mathbf{Z}_p$, $\mathbf{H}_p$ and $\mathbf{U}$ are of size (m_z, n_z), (m_h, n_h) and (m_u, n_u), respectively, regardless of the channel index p. The assumption that sizes of $\mathbf{H}_p$ are equal, is not really restrictive, since any $\mathbf{H}_p$ with a smaller size can be padded with zeros up to the size of the largest one. Clearly, $m_z = m_h + m_u - 1$ and $n_z = n_h + n_u - 1$ if full convolution is considered.

It was mentioned earlier, that an exact solution exists for noise-free MC blind systems (using the subspace method) if certain disparity of channels is guaranteed. The following assumption clarifies the disparity notion and is fundamental to the MC blind deconvolution problem.

Assumption A1: Let $\tilde{H}_p$ be the discrete z-transform of $\mathbf{H}_p$. A set of 2-D polynomials $\{\tilde{H}_p(z_1,z_2), p = 1,\ldots,P\}$ is weakly co-prime.

The polynomials $\tilde{H}_p(z_1,z_2)$ are weakly (factor) co-prime if and only if the greatest common divisor is scalar, i.e., $\tilde{H}_p(z_1,z_2) = C(z_1,z_2)\tilde{H}'_p(z_1,z_2), \forall p = 1,\ldots,P$ hold true only for a scalar factor $C(z_1,z_2) = a$. A similar notion known as strong (zero) co-primeness is defined as follows. The polynomials are strongly co-prime if and only if they do not have common zeros, i.e., there does not exist (ζ_1,ζ_2) : $\tilde{H}_p(\zeta_1,\zeta_2) = 0, \forall p = 1,\ldots,P$. Clearly, both notions are equivalent for 1D polynomials. However, for 2-D polynomials weak co-primeness is much less restrictive than strong co-primeness. Strong co-primeness of two 2-D polynomials is an event of measure zero, since two zero lines on the (z_1,z_2) plane intersect with probability one, but weak co-primeness in practice holds for many common deterministic filters. Strong co-primeness is almost surely satisfied for $P \ge 3$, since three or more zero lines pass through one common point on the (z_1,z_2) plane with probability zero.

The following proposition proved in [26] is regarded as the core stone of the subspace method.

Proposition 1: If $p \ge 2$, A1 holds and $\mathbf{U}$ has at least one nonzero element, then solutions $\{\mathbf{G}_i(m_g,n_g)\}$ to

$$\mathbf{Z}_i * \mathbf{G}_j - \mathbf{Z}_j * \mathbf{G}_i = \mathbf{O}, \quad 1 \le i < j \le P \tag{15}$$

have the form

$$\mathbf{G}_i = \begin{cases} \mathbf{H}_i * \mathbf{K} & \text{for } m_g \geq m_h \wedge n_g \geq n_h \\ \alpha \mathbf{H}_i & \text{for } m_g = m_h \wedge n_g = n_h \\ \emptyset & \text{for } m_g < m_h \vee n_g < n_h \end{cases}$$

where $\mathbf{K}$ is some factor of size $(m_g - m_h + 1, n_g - n_h + 1)$ and α is a scalar.

In the presence of noise, the situation is different and for the correct support (m_h, n_h) system (15) is not equal to zero but rather to some measurement of noise. The strategy in this case is to find the least-squares solution of (15) for $\mathbf{G}_i$. In the framework of our proposed MC blind deconvolution algorithm, we can thus define the regularization of h_p as

$$R(h_1, \ldots, h_P) = \frac{1}{2} \sum_{1 \leq i < j \leq P} \|\mathcal{C}_{z_i}(h_j) - \mathcal{C}_{z_j}(h_i)\|^2 \,, \quad (16)$$

where $\mathcal{C}_{z_i}(\cdot) \equiv (z_i * \cdot)$. It is clear that a correct estimation of the PSF support is crucial, since the support overestimation adds some spurious factor $\mathbf{K}$ to the true solution, and even worth, the support underestimation does not have any solution. It implies, that with respect to (15), the solutions $\mathbf{G}_i$ for different overestimated supports are indistinguishable, i.e., (16) is convex but far from strictly convex. It will be clear later, that the term $\sum_i \|h_i * u - z_i\|^2$ in (4) penalizes the overestimated solutions.

After substituting for R in (4), the Euler-Lagrange equations with respect to h_p are

$$\begin{aligned} &\frac{\partial E}{\partial h_p} = \mathcal{C}_u^*(\mathcal{C}_u(h_p) - z_p) - \gamma \sum_{\substack{i=1 \\ i \neq p}}^{P} \left(\mathcal{C}_{z_i}^* \mathcal{C}_{z_i}(h_p) - \mathcal{C}_{z_i}^* \mathcal{C}_{z_p}(h_i)\right), \\ &\frac{\partial h_p}{\partial n} = 0 \quad \text{on } \partial\Omega \,, \quad p = 1, \ldots, P \,, \end{aligned} \quad (17)$$

where $\mathcal{C}_u(\cdot) \equiv (u * \cdot)$ and the adjoint operator is $\mathcal{C}_u^*(\cdot) = (u(-\mathbf{x}) * \cdot)$. This is a simple set of linear equations and thus finding solutions h_p is a straightforward task. The Neumann boundary condition could be omitted since the support of h_p is assumed to be much smaller then the support of u.

It should be mentioned that Proposition 1 holds only in case that the acquired images $\mathbf{Z}_p$ are of full size, i.e., convolution in (14) is full and thus $\mathbf{Z}_p$ are not cropped. This is, however, seldom true in real applications. For the cropped scenario, a similar proposition holds which is also derived in [26]. We will not discussed this proposition in detail. For our purpose, it will suffice to note that the full convolution operator in (15) must be replaced with a cropped convolution operator. Cropped convolution differs from full convolution only in the size of the definition domain. It is not defined at image boundaries where one of the convolution arguments is not fully defined, i.e., the result of full convolution $\mathbf{Z} * \mathbf{H}$ is of size $(m_z + m_h - 1, n_z + n_h - 1)$, while the result of cropped convolution is of size $(m_z - m_h + 1, n_z - n_h + 1)$ if $m_z \geq m_h$, $n_z \geq n_h$. Cropped convolution is thus well defined even for cropped images and the results of Proposition 1 hold. By using cropped convolution, we get for free another advantage that the Neumann boundary condition in the Euler-Lagrange equation (6) will be automatically satisfied for the convolution term in this equation. A slight computational drawback is the fact that cropped convolution cannot be diagonalized with FT anymore. Nevertheless, we will assume cropped convolution in the following discussion for the reasons given above and show efficient computation of resulting matrices.

IV. MC-AM ALGORITHM

From the above discussion follows that the unveiled energy function E from (4) becomes

$$\begin{aligned} E(u, h_1, \ldots, h_P) = &\frac{1}{2} \sum_{p=1}^{P} \|h_p * u - z_p\|^2 + \\ &\lambda \int_\Omega |\nabla u| + \gamma \frac{1}{2} \sum_{1 \leq i < j \leq P} \|\mathcal{C}_{z_i}(h_j) - \mathcal{C}_{z_j}(h_i)\|^2 \end{aligned} \quad (18)$$

for the TV regularization and we would obtain a similar equation for the Mumford-Shah regularization. Note that $E(u, h_p)$ as a functional of several variables is not convex everywhere and allows infinitely many solutions. If (u, h_p) is a solution, then so are $(\alpha u, \frac{1}{\alpha} h_p)$ (mean-value ambiguity), $(u(\mathbf{x} \pm \xi), h_p(\mathbf{x} \mp \xi))$ (shift ambiguity) for any $\alpha \in \mathbb{R}$ and $\xi \in \mathbb{R}^2$. On the other hand, for fixed u or h_p, $E(u, h_p)$ is a convex functional of h_p or u, respectively. The AM algorithm, for some initial value u^0, alternates between the following two steps:

$$\begin{aligned} h_p^n &= \arg\min_{h_p} E(u^{n-1}, h_p) \quad \text{by (17)} \\ u^n &= \arg\min_{u} E(u, h_p^n) \quad \text{by (8) or (13)} \end{aligned} \quad (19)$$

for $n \geq 1$. A minimizer of the first minimization equation can be determined by directly solving $\frac{\partial E}{\partial h_p} = 0$, i.e., equation (17). The second minimization equation can be solved via (8) if the TV functional is considered or via (13) if the Mumford-Shah functional is considered. The mean-value ambiguity is removed by constraint (3). It will be explained at the end of this section, that this constraint is automatically satisfied in the AM algorithm. A correct setting of the blur size (m_h, n_h) alleviates the shift ambiquity. In the noise-free case, the AM algorithm transforms into the EVAM method: the first step in (19) becomes perfect blur restoration and the second step calculates the least-squares solution of the image. When noise is present, any convergence analysis is difficult to carry out but results of our experiments are satisfying and illustrate a strong stability of the algorithm.

Consider the discretization scheme described in Section II. The P-channel acquisition model (1) becomes in the discrete space

$$\mathbf{z} = \mathcal{H}\mathbf{u} + \mathbf{n} = \mathcal{U}\mathbf{h} + \mathbf{n} \,, \quad (20)$$

where $\mathbf{h} = [\mathbf{h}_1^T, \ldots, \mathbf{h}_P^T]^T$ and $\mathbf{z} = [\mathbf{z}_1^T, \ldots, \mathbf{z}_P^T]^T$ denote vectors of size Pm_hn_h and Pm_zn_z representing discrete, concatenated and lexicographically ordered h_p and z_p, respectively. Matrices $\mathcal{U}$ and $\mathcal{H}$ are defined as

$$\mathcal{U} \equiv \underbrace{\begin{pmatrix} \mathbf{C_U} & & \mathbf{0} \\ & \ddots & \\ \mathbf{0} & & \mathbf{C_U} \end{pmatrix}}_{P}, \quad \mathcal{H} \equiv \begin{pmatrix} \mathbf{C_{H_1}} \\ \vdots \\ \mathbf{C_{H_P}} \end{pmatrix}, \quad (21)$$

$$\frac{1}{2}\sum_{i=1}^{m}\sum_{j=1}^{n}\left(v_{i+\frac{1}{2},j}|u_{i+1,j}-u_{i,j}|^2+v_{i,j+\frac{1}{2}}|u_{i,j+1}-u_{i,j}|^2+\frac{1}{v_{i+\frac{1}{2},j}}+\frac{1}{v_{i,j+\frac{1}{2}}}\right)\equiv\frac{1}{2}\mathbf{u}^T\mathcal{L}_4(v)\mathbf{u}+c(v) \tag{23}$$

$$\begin{aligned}\frac{1}{2}\sum_{i=1}^{m}\sum_{j=1}^{n}\Bigg(&v_{i+\frac{1}{2},j}|u_{i+1,j}-u_{i,j}|^2+v_{i,j+\frac{1}{2}}|u_{i,j+1}-u_{i,j}|^2+\frac{1}{\sqrt{2}}v_{i+\frac{1}{2},j+\frac{1}{2}}|u_{i+1,j+1}-u_{i,j}|^2\\&+\frac{1}{\sqrt{2}}v_{i+\frac{1}{2},j-\frac{1}{2}}|u_{i+1,j-1}-u_{i,j}|^2+\frac{1}{v_{i+\frac{1}{2},j}}+\frac{1}{v_{i,j+\frac{1}{2}}}+\frac{1}{v_{i+\frac{1}{2},j+\frac{1}{2}}}+\frac{1}{v_{i+\frac{1}{2},j-\frac{1}{2}}}\Bigg)\equiv\frac{1}{2}\mathbf{u}^T\mathcal{L}_8(v)\mathbf{u}+c(v)\,,\end{aligned} \tag{24}$$

where $\mathbf{C_U}$ and $\mathbf{C_{H}}_p$ denote cropped convolution with $\mathbf{U}$ and $\mathbf{H}_p$, respectively. The size of $\mathcal{U}$ is (Pm_zn_z, Pm_hn_h) and of $\mathcal{H}$ is (Pm_zn_z, m_un_u). If the size of the recorded images is (m_z, n_z) then the minimum size of the original image is $m_u = m_z + m_h - 1$, $n_u = n_z + n_h - 1$.

Suppose that $\mathcal{Z}$ is a matrix defined by the iterative prescription

$$\begin{aligned}\mathbf{S}_{P-1}&\equiv\begin{pmatrix}\mathbf{C}_{\mathbf{Z}_P} & -\mathbf{C}_{\mathbf{Z}_{P-1}}\end{pmatrix},\\ \mathbf{S}_t&\equiv\left(\begin{array}{c|c}\begin{matrix}\mathbf{C}_{\mathbf{Z}_{t+1}}\\ \mathbf{C}_{\mathbf{Z}_{t+2}}\\ \vdots\\ \mathbf{C}_{\mathbf{Z}_P}\end{matrix} & \begin{matrix}-\mathbf{C}_{\mathbf{Z}_t} & & \\ & -\mathbf{C}_{\mathbf{Z}_t} & \\ & & \ddots \\ & & & -\mathbf{C}_{\mathbf{Z}_t}\end{matrix}\\ \hline \mathbf{O} & \mathbf{S}_{t+1}\end{array}\right)\\ &t = P-2, P-3, \ldots, 1\,,\\ \mathcal{Z}&\equiv\mathbf{S}_1\,,\end{aligned} \tag{22}$$

where $\mathbf{C}_{\mathbf{Z}_t}$ denotes cropped convolution with the image $\mathbf{Z}_t$, then the right-hand side of (16) becomes $\frac{1}{2}\|\mathcal{Z}\mathbf{h}\|^2$ and the size of $\mathcal{Z}$ is $(\frac{P(P-1)}{2}(m_z-m_h+1)(n_z-n_h+1), Pm_hn_h)$. We assume that $\mathrm{supp}(\mathbf{Z}_p) \gg \mathrm{supp}(\mathbf{H}_p)$ for $p = 1, \ldots, P$. From Proposition 1 follows, that for the noise-free case, $\mathcal{Z}$ has full column rank ($\mathrm{rank}(\mathcal{Z}) = Pm_hn_h$) only if the blur size is underestimated, i.e $m_h < m_h^* \vee n_h < n_h^*$, where (m_h^*, n_h^*) is the correct blur size. For the overestimated blur size $m_h \geq m_h^* \wedge n_h \geq n_h^*$, $\mathrm{rank}(\mathcal{Z}) = Pm_hn_h - (m_h - m_h^* + 1)(n_h - n_h^* + 1)$.

In case of the modified TV functional (7), we need to consider the discretization scheme of the flux variable v. For the simple four–connectivity approximation, one obtains (23) and for the more elaborated eight–connectivity approximation (24), where both $\mathcal{L}_4$ and $\mathcal{L}_8$ are block tridiagonal matrices formed from $v_{i\pm1/2,j\pm1/2}$ and $c(v)$ is a sum of inverse values of v. More precisely, the diagonal blocks are tridiagonal in both $\mathcal{L}$'s, and the off-diagonal blocks in $\mathcal{L}_4$ are just diagonal matrices, while in $\mathcal{L}_8$ they are tridiagonal as well. Almost identical discrete equations can be obtained for the Mumford-Shah regularization by means of (12). For instance, if $\phi \equiv 0$ except for $\xi \in \{(0,1),(1,0),(0,-1)(-1,0)\}$ where $\phi(\xi) = 1/2$ then (12) takes the form of (23) and, if in addition, $\phi(\eta) = 1/(2\sqrt{2})$ for $\eta \in \{(1,1),(-1,-1),(1,-1),(-1,1)\}$ then (12) takes the form of (24). We should not forget, however, that the difference between TV and Mumford-Shah still resides in the calculation of the flux variable $v = \varphi(u)$, e.g., from (8) follows that for TV

$$v_{i\pm1/2,j\pm1/2} = \min(\max(\epsilon, 1/|u_{i\pm1,j\pm1} - u_{i,j}|), 1/\epsilon)\,, \tag{25}$$

and from (13) for Mumford-Shah

$$v_{i\pm1/2,j\pm1/2} = \frac{1}{1+\left(\frac{\pi(u_{i\pm1,j\pm1}-u_{i,j})^2}{2\mu}\right)^2}\,. \tag{26}$$

In the vector-matrix notation, the total energy function (18) for some overestimated blur size (m_h, n_h) is

$$E_{(m_h,n_h)}(\mathbf{u},\mathbf{h}) = \lambda\mathbf{u}^T\mathcal{L}\mathbf{u} + \gamma\|\mathcal{Z}\mathbf{h}\|^2 + \|\mathcal{H}\mathbf{u}-\mathbf{z}\|^2\,, \tag{27}$$

where $\mathcal{L}$ stands for $\mathcal{L}_4$, $\mathcal{L}_8$, or any other matrix of similar form resulting from a different approximation. The flux variable v is neglected to simplify notation. Using this equation, the minimization algorithm in (19) reduces to a sequence of solutions of simple linear equations. The discrete MC-AM algorithm thus consist of the following steps:

Require: initial value $\mathbf{u}^0$, blur size (m_h, n_h), where $m_h > m_h^*, n_h > n_h^*$, and regularization parameters $\gamma > 0$ and $\lambda > 0$

1: **for** $n \geq 1$ **do**
2: $\quad\mathbf{h}^n \leftarrow$ solve $[(\mathcal{U}^{n-1})^T\mathcal{U}^{n-1} + \gamma\mathcal{Z}^T\mathcal{Z}]\mathbf{h}^n = (\mathcal{U}^{n-1})^T\mathbf{z}$, $\{\mathcal{U}^{n-1}$ is constructed by $\mathbf{u}^{n-1}\}$
3: $\quad$set $\mathbf{g}^0 = \mathbf{u}^{n-1}$ and $v^0 = \varphi(\mathbf{u}^{n-1})$
4: $\quad$**for** $k \geq 1$ **do**
5: $\quad\quad\mathbf{g}^k \leftarrow$ solve $[(\mathcal{H}^n)^T\mathcal{H}^n + \lambda\mathcal{L}(v^{k-1})]\mathbf{g}^k = (\mathcal{H}^n)^T\mathbf{z}$, $\{\mathcal{H}^n$ is constructed by $\mathbf{h}^n\}$
6: $\quad\quad v^k = \varphi(\mathbf{g}^k)$, {for φ use (25) or (26)}
7: $\quad$**end for**
8: $\quad\mathbf{u}^n \leftarrow \mathbf{g}^k$
9: **end for**

The linear equation at line 2 can be solved directly since the symmetric square matrix $[(\mathcal{U}^{n-1})^T\mathcal{U}^{n-1} + \gamma\mathcal{Z}^T\mathcal{Z}]$ is of relatively small size Pm_hn_h, and is almost surly regular due to full column rank of the convolution matrix $\mathcal{U}$. Any reasonable image u is "persistently exciting", i.e., $u * h \neq 0$ for every FIR filter h of size much smaller than u. It was already mentioned that for the noise-free case, the dimension of the null space of $\mathcal{Z}$ is proportional to the overestimated blur size (m_h, n_h), more precisely the dimension is equal to $(m_h - m_h^* + 1)(n_h - n_h^* + 1)$, and any $\mathbf{g} \in \mathrm{null}(\mathcal{Z})$ takes the form $\mathbf{g} = [\mathrm{vec}\{\mathbf{K} * \mathbf{H}_1\}^T, \ldots, \mathrm{vec}\{\mathbf{K} * \mathbf{H}_P\}^T]$, where $\mathbf{K}$ is some spurious factor and $\mathbf{H}_p$ are correct PSF's of size (m_h^*, n_h^*). The spurious factor spoils the correct solution but cannot be avoided if the exact size of blurs is

not known in advance and if only $\mathcal{Z}$ is considered. It is the fundamental constraint (2) included at line 2 which penalizes the spurious factor. To see this, consider $\min_n \sum_i \|\mathbf{U}^n * \mathbf{K} * \mathbf{H}_i - \mathbf{U} * \mathbf{H}_i\|^2$ which is strictly greater than zero, unless $\mathbf{K}$ is a factor of $\mathbf{U}$, which cannot happen almost surely. Hence, the minimum is reached only for $\mathbf{U}^n = \mathbf{U}$ and $\mathbf{K}$ reduced to the 2D delta function.

Due to the large size of each matrix, it is not feasible to compute the products $\mathcal{U}^T\mathcal{U}$ and $\mathcal{Z}^T\mathcal{Z}$ by first constructing $\mathcal{U}$ and $\mathcal{Z}$ and then doing the matrix multiplication. Fortunately, there exists a very fast direct construction method for both products. Moreover, the latter product is constructed only once at the beginning. It is easy to observe that the products consist of P^2 square blocks $\mathbf{B}_{ij}$ of size $m_h n_h$, $i, j = 1, \ldots, P$. In case of $\mathcal{U}^T\mathcal{U}$, only the diagonal blocks are nonzero and defined as $\mathbf{B}_{ii} = {\mathbf{C}_\mathbf{U}}^T\mathbf{C}_\mathbf{U}$. In case of $\mathcal{Z}^T\mathcal{Z}$, the off-diagonal blocks are defined as $\mathbf{B}_{ij} = -\mathbf{C}^T_{\mathbf{Z}_j}\mathbf{C}_{\mathbf{Z}_i}$ and the diagonal blocks $\mathbf{B}_{ii} = \sum_{k\neq i} \mathbf{C}^T_{\mathbf{Z}_k}\mathbf{C}_{\mathbf{Z}_k}$. We assume that $\mathbf{C}$ denotes cropped convolution. After some consideration, one would derive that the elements of $\mathbf{B}_{ij}$ are calculated as $b^{ij}_{kl} = \sum_{m=1}^{m_z-m_h+1}\sum_{n=1}^{n_z-n_h+1} z_i(m+\mu(l), n+\nu(l))z_j(m+\mu(k), n+\nu(k))$, where z_i and z_j are elements of $\mathbf{Z}_i$ and $\mathbf{Z}_j$, respectively, and index shifts are $\mu(k) = [(k-1) \mod m_h]$, $\nu(k) = \left\lfloor \frac{k-1}{m_h} \right\rfloor$. Likewise, if z_i, z_j are replaced with u we get the elements of the diagonal blocks in $\mathcal{U}^T\mathcal{U}$. This way, one block is computed in $O((m_h n_h)m_z n_z \log(m_z n_z))$ multiplies. On contrary, the full matrix multiplication requires $O((Pm_h n_h)^2 m_z n_z)$ multiplies.

The second linear equation at line 5 contains the symmetric positive semidefinite matrix $[(\mathcal{H}^n)^T\mathcal{H}^n + \lambda\mathcal{L}(v^{k-1})]$ of size $m_u n_u$. Most of the common PSF's have zeros in the frequency domain and/or very small values at higher frequencies and the resulting convolution matrices $\mathcal{H}$ are strongly ill-conditioned. Hence, the problem at line 5 is ill-posed and contains too many unknowns to be solvable by direct methods. A common approach, which we have also adopted, is to use conjugate gradient (CG) or preconditioned CG methods, see [5], [31]. The flux variable v is calculated directly by means of (25) if TV is considered or by means of (26) if Mumford-Shah regularization is considered. The relaxation parameter ϵ in (25) influences both the converge speed of the algorithm and accuracy of solutions at line 5. Refer to [4] for a discussion about how ϵ alters the convergence rate and for comparison of different numerical methods. In our experiments, we have found values around 10^{-3} the most appropriate. The parameter μ in (26) acts as a weighting factor of the discontinuity term in the Mumford-Shah functional (9). There is no straightforward estimation of the parameter's correct value and an evaluation by trial and error is probably the only choice. In our implementation, we alternate between minimizations over $\mathbf{g}$ and v only five times before returning back to line 2.

A. Convergence properties

Convergence of the algorithm cannot be fully resolved on a purely theoretical basis. Nevertheless, we have made several interesting observations that rely on the fact that cropped convolution can be approximated by circular convolution and that eigenvalues of a circular convolution matrix are Fourier coefficients of the convolution mask.

Constraint (3), which was left aside at the beginning, is automatically satisfied in the algorithm if the mean values of the acquired images $\mathbf{z}_p$ and the initial estimate $\mathbf{u}^0$ are all equal, i.e., $\bar{\mathbf{u}}^0 = \bar{\mathbf{z}}_1 = \ldots = \bar{\mathbf{z}}_P$. To see this, we first approximate at line 2 cropped convolution with circular convolution and then apply FT to the equation. From the definition of $\mathcal{Z}$ in (22) and from the assumption of zero-mean noise follow, that the transformed $\mathcal{Z}^T\mathcal{Z}$ vanishes at the spatial frequency $(0,0)$. Since the $(0,0)$ frequencies refer to mean values, according to the the definition of FT, the solution $\mathbf{h}^n$ satisfies $\bar{\mathbf{h}}^n_p = 1$ if $\bar{\mathbf{u}}^{n-1} = \bar{\mathbf{z}}_p$. Likewise, if $\bar{h}^n_p = 1$, the solution $\mathbf{g}^k$ at line 5 satisfies $\bar{\mathbf{g}}^k = \frac{1}{P}\sum_{p=1}^P \bar{\mathbf{z}}_p = \bar{\mathbf{z}}_p$, since $\mathcal{L}(v^{k-1})$ has zero column-wise sums and hence vanishes at spatial frequencies $(0,\cdot)$ and $(\cdot,0)$.

The AM algorithm is a variation on the steepest-descent algorithm. Our search space is a concatenation of the blur subspace and the image subspace. The algorithm first descends in the blur subspace and after reaching the minimum, i.e., $\nabla_\mathbf{h} E = 0$, it advances in the image subspace in the direction $\nabla_\mathbf{u} E$ orthogonal to the previous one, and this scheme repeats. To speedup the minimization, one may be tempted to implement direct set methods like Powell's that descend in arbitrary directions but this would require to solve nonlinear equations and the efficiency of such approach becomes problematic. Convergence is assured if the descent is restricted to a convex region of the functional which means that the Hessian matrix is positive semidefinite in the region. The Hessian of $E(\mathbf{u},\mathbf{h})$ is a symmetric matrix $\begin{pmatrix} \nabla_{\mathbf{hh}} & \nabla_{\mathbf{hu}} \\ \nabla^T_{\mathbf{hu}} & \nabla_{\mathbf{uu}} \end{pmatrix}$, where $\nabla_{\mathbf{hh}} = \mathcal{U}^T\mathcal{U} + \gamma\mathcal{Z}^T\mathcal{Z}$, $\nabla_{\mathbf{uu}} = \mathcal{H}^T\mathcal{H} + \lambda\mathcal{L}$ and the cross second derivative $\nabla_{\mathbf{hu}}$ is a combination of convolution and correlation matrices with $\mathbf{u}$, $\mathbf{h}$, $\mathbf{z}$. Let $\nabla_{\mathbf{hh}}$ and $\nabla_{\mathbf{uu}}$ be positive definite, which is true if $\mathbf{u}$ is persistently exciting and $\mathbf{h}_p$ are strongly coprime. The Hessian is then positive semidefinite if and only if $(\mathbf{x}^T\nabla_{\mathbf{hh}}\mathbf{x})(\mathbf{y}^T\nabla_{\mathbf{uu}}\mathbf{y}) \geq |\mathbf{x}^T\nabla_{\mathbf{hu}}\mathbf{y}|^2$ for all $\mathbf{x} \in \mathbb{R}^{Pm_h n_h}$ and all $\mathbf{y} \in \mathbb{R}^{m_u n_u}$. If we assume that the convolution matrices can be block diagonalized with FT then the above semidefinite condition is satisfied if is satisfied for each spatial frequency alone. The multichannel term $\gamma\mathcal{Z}^T\mathcal{Z}$ is singular for each frequency and can be thus omitted. This leads us to a conclusion that this multichannel term does not directly enlarge the region of convexity. Instead, by defining mutual relations between the channel blurs, it penalizes any diversion of one blur from the rest. The necessary condition of convexity is thus expressed for each spatial frequency in each channel as $|\tilde{u}|^2(|\tilde{h}|^2 + \lambda|\tilde{l}|^2) \geq |\tilde{u}\tilde{h} + \tilde{u}\tilde{h}^* - \tilde{z}|^2$, where $\tilde{(\cdot)}$ denotes a Fourier coefficient of the corresponding signal, $\tilde{l}$ is a simplified expression that approximates eigenvalues of $\mathcal{L}$. Fundamental constraint (2) for a zero noise level takes the form $\tilde{u}\tilde{h} = \tilde{z}$ in the Fourier domain. After substituting the constraint into the above condition, we get $|\tilde{u}|^2(|\tilde{h}|^2 + \lambda|\tilde{l}|^2) \geq |\tilde{u}|^2|\tilde{h}|^2$ which is always true. In general, the condition is not satisfied only for the fundamental constraint but generates a periodic manifold that is difficult to visualize. It is important to note that the manifold size grows with λ, i.e., with increasing noise,

convexity is guaranteed on a larger neighborhood of $\tilde{u}\tilde{h} = \tilde{z}$.

B. Estimations of parameters γ and λ

To calculate precisely the regularization parameters is not only a tedious task but it also gives results that are of not much help in practical applications, since both parameters depend on a noise level which we usually do not know. Expressions derived here are very loose approximations that do not provide exact values but rather give a hint on the mutual relation of the parameters. Consider the equation at line 2 and let the values of $\mathbf{u}$ and $\mathbf{h}$ be equal to the original image and correct PSF's, respectively. Under the squared L^2 norm, we obtain $\|\mathcal{U}^T(\mathcal{U}\mathbf{h}-\mathbf{z})\|^2 = \gamma^2\|\mathcal{Z}^T\mathcal{Z}\mathbf{h}\|^2$, where $\|\mathcal{U}\mathbf{h}-\mathbf{z}\|^2 = \|\mathbf{n}\|^2 \approx Pm_z n_z\sigma^2$. It is easy to verify that, if $\mathbf{n}$ is white Gaussian noise and $\mathcal{U}$ denotes convolution with $\mathbf{u}$, $\|\mathcal{U}^T(\mathcal{U}\mathbf{h}-\mathbf{z})\|^2 \approx Pm_h n_h\|\mathbf{u}\|^2\sigma^2$. Since $\mathbf{h}$ stands for the correct PSF's, it must be a linear combination of $\mathcal{Z}^T\mathcal{Z}$ eigenvectors that correspond to a cluster of minimum eigenvalues. Hence, $\|\mathcal{Z}^T\mathcal{Z}\mathbf{h}\|^2 = \lambda_1^2\|\mathbf{h}\|^2$, where λ_1 denotes the minimum eigenvalue of $\mathcal{Z}^T\mathcal{Z}$. From the definition of $\mathcal{Z}$ and Proposition 1 follow that $\lambda_1 \approx \sigma^2(P-1)m_u n_u$. Finally, we get the approximation

$$|\gamma| \approx \frac{1}{P-1}\frac{\sqrt{Pm_h n_h}}{\|\mathbf{h}\|}\frac{\|\mathbf{u}\|}{m_u n_u}\frac{1}{\sigma}\,. \tag{28}$$

The L^2 norms of $\mathbf{u}$ and $\mathbf{h}$ are of course not known in advance but $\|\mathbf{u}\|$ can be successfully approximated by $\|\mathbf{z}_p\|$ and if $\mathbf{h} > 0$ then $\frac{P}{m_h n_h} \le \|\mathbf{h}\|^2 \le P$.

If we apply a similar procedure to the equation at line 5, we derive only the bottom limit of the regularization parameter λ. The uncertainty resides in the term $\|\mathcal{L}\mathbf{u}\|^2$, which cannot be simplified, since it totally depends on local behavior of the image function u. We may only formulate a generous upper limit which is $\|\mathcal{L}\mathbf{u}\|^2 \le c^2\|\mathbf{u}\|^2$, where the constant c depends on the used approximation and the regularization term, i.e, for TV with $\mathcal{L}_4$, $c_4 = 4$ and for TV with $\mathcal{L}_8$, $c_8 = 4 + 4\frac{1}{\sqrt{2}}$. The bottom limit is in general zero. Now, since $\|\mathcal{H}^T(\mathcal{H}\mathbf{u}-\mathbf{z})\|^2 \approx \|\mathbf{h}\|^2\sigma^2 m_u n_u$, we obtain the approximated bottom limit of λ as

$$|\lambda| \gtrapprox \frac{\|\mathbf{h}\|\sigma}{c}\frac{\sqrt{m_u n_u}}{\|\mathbf{u}\|} \tag{29}$$

The product of the parameters

$$|\gamma||\lambda| \ge \frac{1}{c(P-1)}\sqrt{\frac{Pm_h n_h}{m_u n_u}} \tag{30}$$

depends only on the dimensions of the problem and thus defines a fix relation between the parameters.

V. Experimental results

In this section, we demonstrate the performance of our MC-AM approach on three different sets of data: simulated, real indoor and astronomical data. First, the simulated data for different SNR are used to compare results of MC-AM and EVAM. Second, the performance of MC-AM is evaluated on out-of-focus data acquired by a standard commercial digital camera. Last but not least, we demonstrate capabilities of the MC-AM approach on data from astronomical ground-based observations of the Sun.

For the evaluation of the simulated data, we use the percentage mean squared errors of the estimated PSF's $\hat{\mathbf{h}}$ and of the estimated original image $\hat{\mathbf{u}}$, respectively, defined as follows:

$$\begin{aligned}\mathrm{PMSE}(\mathbf{u}) &\equiv 100\frac{\|\hat{\mathbf{u}}-\mathbf{u}\|}{\|\mathbf{u}\|}\,,\\ \mathrm{PMSE}(\mathbf{h}) &\equiv 100\frac{\|\hat{\mathbf{h}}-\mathbf{h}\|}{\|\mathbf{h}\|}\,.\end{aligned} \tag{31}$$

Both $\hat{\mathbf{u}}$ and $\hat{\mathbf{h}}$ are the outputs of MC-AM. In general, the mean squared errors do not correspond to our visual evaluation of image quality and visual comparison is often the only reliable evaluation technique. Nevertheless, the mean squared errors give us a hint how successful the restoration task was and therefore we present the calculated errors together with estimated images. In cases of the camera and astronomical data, we use a wavelet-based focus measure [32] to compare results. It is necessary to remark that all the focus measures, which have been proposed in the literature, are easily deceived by possible artifacts which often occur in the reconstruction process. Artifacts are features (details) that were not present in original images and have been added to the images later due to erroneous image processing.

All the experiments were conducted for the TV regularization with the eight–connectivity discretization scheme. The Mumford-Shah regularization was found to produce similar results with one advantage of having a good edge detector in the flux variable v. Less advantages is the presence of the new parameter μ which influences the amount of edges. Since we were not interested in segmentation properties of the Mumford-Shah functional, the flexibility provided by μ was redundant.

A. Simulated data

Cameraman image of size 100×100 in Fig. 1(a) was first convolved with three 7×7 masks in Fig. 1(b) and then white Gaussian noise at five different levels (SNR = 50, 40, 30, 20, and 10 dB) was added. This way we simulated three acquisition channels ($P = 3$) with a variable noise level that produced a series of degraded images $\mathbf{z}_1$, $\mathbf{z}_2$ and $\mathbf{z}_3$. The signal-to-noise ratio is calculated as usual

$$\mathrm{SNR} = 10\log\left(\frac{\sum_{i=1}^{P}\|\mathbf{z}_i - \bar{\mathbf{z}}_i\|^2}{Pm_z n_z\sigma^2}\right)\,. \tag{32}$$

Both algorithms, our MC-AM and Harikumar's EVAM, were applied to the degraded data. The MC-AM algorithm was let to iterate over the main loop (lines 1 to 9) ten times, and within each iteration, the inner loop (lines 4 to 7) was iterated five times. The input parameters were initialized as follows: $\mathbf{u}^0 = \sum_{i=1}^{P}\mathbf{z}_i/P$; $(m_h, n_h) = (7, 7)$; λ was calculated from (29), since we know σ; and γ was estimated from the parameter product (30). Results for $\mathrm{SNR} = 50$dB, $\mathrm{SNR} = 40$dB, and $\mathrm{SNR} = 30$dB are shown in Figs. 2, 3, and 4, respectively. Noise gets amplified in the EVAM reconstruction since it is not considered in the derivation of this method. The results for $\mathrm{SNR} = 30$dB illustrate vividly this drawback. On contrary, the MC-AM algorithm is still stable even for lower SNR's (20dB,

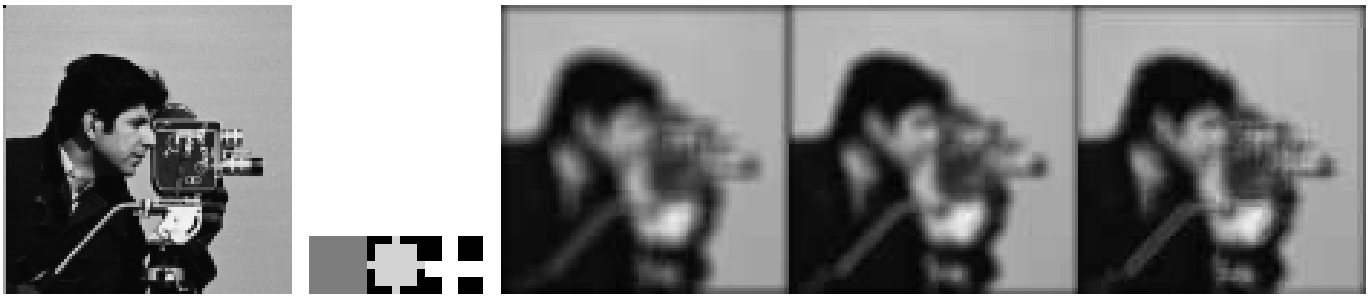

(a) (b) (c)

Fig. 1. (a) original 100×100 cameraman image used for simulations; (b) three 7×7 convolution masks; (c) blurred and noise-free images

(a) (b) (c)

Fig. 2. Estimation of the cameraman image and blurs from three $\mathrm{SNR} = 50$dB degraded images ((a) degradation with $\mathbf{h}_1$) using (b) the MC-AM algorithm and (c) the EVAM algorithm.

(a) (b) (c)

Fig. 3. Estimation of the cameraman image and blurs from three $\mathrm{SNR} = 40$dB degraded images ((a) degradation with $\mathbf{h}_1$) using (b) the MC-AM algorithm and (c) the EVAM algorithm.

10dB) as Fig. 5 demonstrates. The percentage mean squared errors of the results are summarized in Table I.

B. Real indoor data

Four images of a flat scene were acquired with a standard digital camera focused to 80 (objects in focus), 40, 39, and 38cm distance, respectively. The aperture was set at F2.8 and the exposure at $1/320$s. The acquired data were stored as low resolution 480×640 24-bit color images and only the central rectangular part of the green channel of size 200×250 was considered for reconstruction. The central part of the first image, which captures the scene in focus, is shown in Fig. 6(a). Three remaining images, Fig. 6(c), were used as the input for the MC-AM algorithm. The parameter $\lambda = 1.6 \times 10^{-4}$ was estimated experimentally by running the algorithm with different λ's and selecting the most visually acceptable results. The parameter γ was calculated from (30). A defocused camera causes image degradation that is modeled

(a) (b) (c)

Fig. 4. Estimation of the cameraman image and blurs from three $\mathrm{SNR} = 30$dB degraded images ((a) degradation with $\mathbf{h}_1$) using (b) the MC-AM algorithm and (c) the EVAM algorithm.

(a) (b) (c) (d)

Fig. 5. Estimation of the cameraman image and blurs from degraded images with low SNR using the MC-AM algorithm; (a)-(b) $\mathbf{h}_1$ degraded image with $\mathrm{SNR} = 20$dB and restored image-blur pair; (c)-(d) $\mathbf{h}_1$ degraded image with $\mathrm{SNR} = 10$dB and restored image-blur pair.

TABLE I
PERFORMANCE OF THE EVAM AND MC-AM ALGORITHMS ON SYNTHETIC DATA IN FIG.1.

SNR	EVAM		MC-AM	
	PMSE($\mathbf{h}$)	PMSE($\mathbf{u}$)	PMSE($\mathbf{h}$)	PMSE($\mathbf{u}$)
50dB	2.15	2.31	3.12	2.29
40dB	6.33	6.90	7.95	4.04
30dB	51.75	20.92	15.25	7.03
20dB	n/a	n/a	27.3	12.93
10dB	n/a	n/a	44.88	21.86

by cylindrical blurs. A cepstrum analysis [33] was used to estimate diameters of these blurs, which were determined to be around 8 pixels. The size of blurs was then enlarged to 10×10 to assure inclusion of the whole cylinder. Obtained results after 10 iterations are shown in Fig. 6(b). Further iterations did not produce any visual enhancement. Simple visual comparison reveals that the letters printed on book covers are more readable in the restored image but still lack the clarity of the focused image, and that the reconstructed blurs resemble the cylindrical blurs as it was expected.

A quantitative evaluation of the amount of image blurring was done by wavelet-based focus measure [32]. The measured values, which rate the focus or the sharpness of images, are summarized in Table II. The three defocused images differ only slightly from each other and the difference is not visually detectable. However, the focus measure was able to distinguish different focus levels. It decreases as the difference from the correct focus distance increases. The focus measure of the restored image is significantly higher than the measures of the input images. It is remarkable how successful the restoration was, since one would expect that the similarity of blurs will violate the co-primeness assumption. It is believed that the algorithm would perform even better if a wider disparity between blurs was assured. Another interesting observation is the fact that the restored image gives a smaller response than the focused image. This is of course in agreement with our visual evaluation but it also supports a hypothesis that our restoration technique produces only few artifacts.

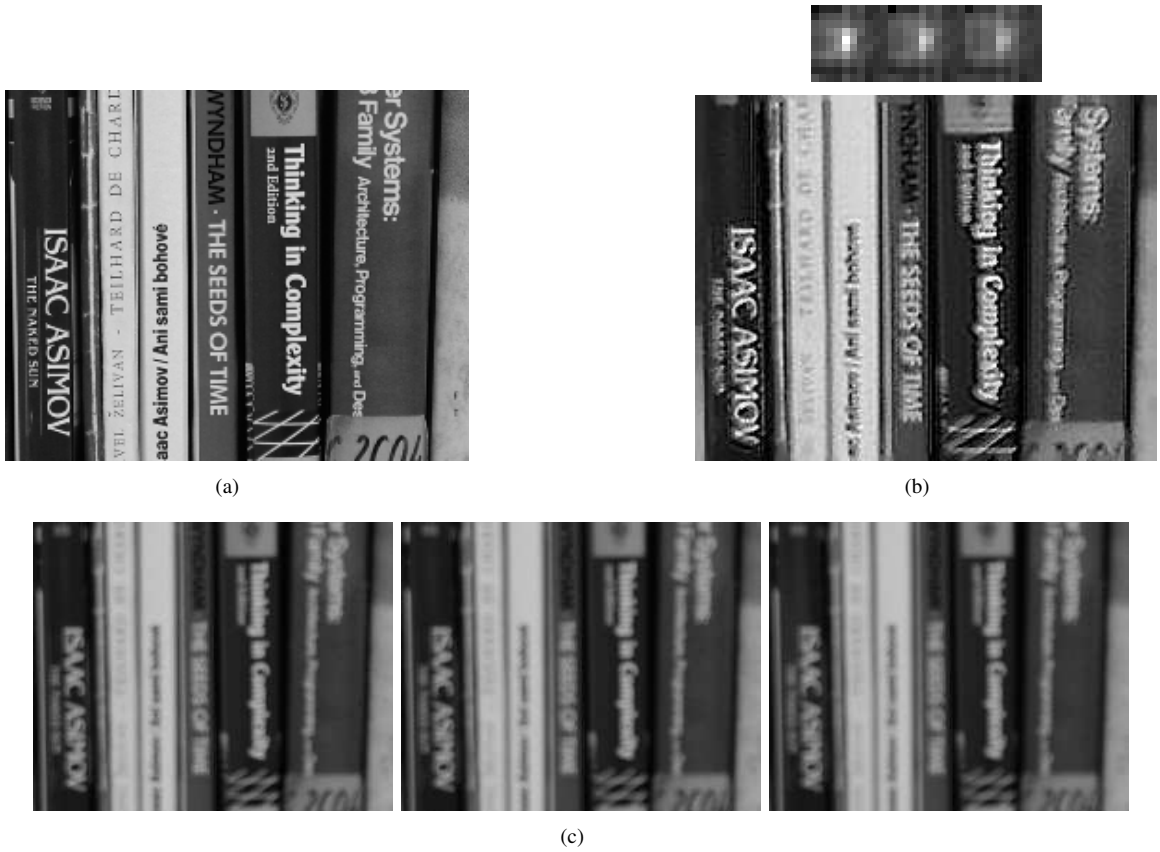

Fig. 6. Real indoor images: (a) 200×250 image acquired with the digital camera set to the correct focus distance of 80cm; (b) MC-AM estimated image and 10×10 blurs obtained from three images (c) of false focus distances 40cm, 39cm and 38cm, after 10 iterations and $\lambda = 1.6 \times 10^{-4}$.

TABLE II
FOCUS MEASURES CALCULATED FOR THE REAL INDOOR IMAGES IN FIG. 6

Image (focus distance)	focused (80cm)	out of focus (40cm)	out of focus (39cm)	out of focus (38cm)	restored
Focus Measure	0.3040	0.1064	0.0947	0.0859	0.2494

C. Astronomical data

The last test which we have conducted was on real astronomical data obtained in the observation of the Sun. In the ground-based observations, the short-exposure images from the telescope are corrupted by "seeing". This degradation leads to image blurring, where the actual PSF is a composition of the intrinsic PSF of the telescope (which is constant over the observation period) and of a random component describing the perturbations of the wavefronts in the Earth's atmosphere. Different parts of the solar atmosphere are observed in different spectral bands. The lower part called photosphere is usually observed in visible light of $\lambda = 590$ nm while the medium part called chromosphere is best to observe in H_α ($\lambda = 656.3$ nm) wavelength. In visible light the effects of fluctuations in the refractive index of the air caused by temperature variations are more significant than in H_α. Since the atmospheric conditions may change very quickly, the acquired image sequence usually contains images of different quality from almost sharp to heavy blurred ones. Such sequence, which is a result of one observation session, may consist of several tens (or even hundreds) of images. Multichannel blind deconvolution is the way how to fuse the individual images of low quality to obtain one (or a few) "optimal" images which can be used for further investigation of astronomical phenomena.

In this experiment, we processed a sequence of images of a sunspot. Since the images were taken shortly one after another they are almost perfectly registered. The random nature of the atmospheric turbulence provides the necessary co-primeness of the individual PSF's. The least degraded image from the sequence, which is shown in Fig. 7(a), was selected as a reference image. Two other images of medium degradation, Figs. 7(b) and 7(c), were used as the input of the algorithm. The size of blurring masks was set to 12×12 which was believed to be large enough to contain the original blurring functions. The parameter λ was set to 10^{-4} which corresponds to $\mathrm{SNR} \approx 40$dB and which is the expected noise level for this type of images. The restored image in Fig. 8 was obtained after 3 iterations of the MC-AM algorithm. It is worth noting that the used data are far from being "ideal" for the application of the MC-AM algorithm – there are only two channels, and their degradations are of similar nature. Nevertheless, the results are encouraging. By visual assessment, the restored image is clearly sharper than the two input images, contains no (or few) artifacts and its quality is comparable to the reference image. As in the previous experiment, we asses the quality also by quantitative focus measure (see Table III). The focus measure of the restored image is significantly higher than that of the

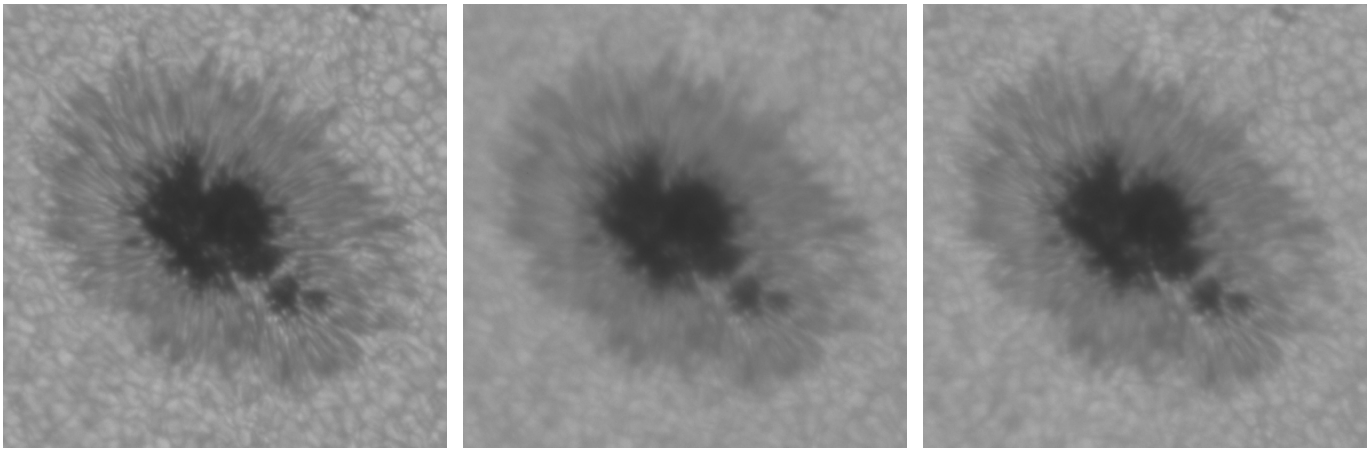

(a) (b) (c)

Fig. 7. Astronomical data: (a) the least degraded 500×500 image of the sunspot from the sequence acquired with the terrestrial telescope (reference); (b)-(c) two blurred images from the sequence used for the reconstruction.

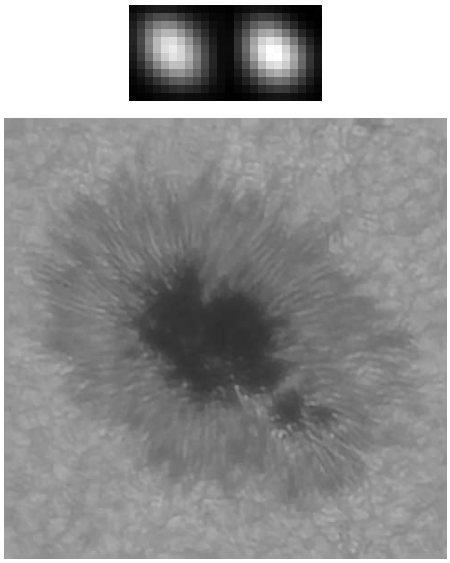

Fig. 8. Astronomical data: MC-AM reconstructed sunspot and 12×12 blurs with $\lambda = 10^{-4}$.

TABLE III
FOCUS MEASURES CALCULATED FOR THE SUNSPOT IMAGES IN FIGS. 7 AND 8

Image	reference	2 blurred (input)		restored (output)
Focus Measure	0.0149	0.0102	0.0112	0.0184

input images and even slightly higher than the measure of the reference image. Along with the visual assessment, this illustrates a good performance of our method in this case.

VI. CONCLUSION

We have developed the algorithm for multichannel blind image restoration which combines the benefits of the edge preserving denoising techniques and the one-step subspace (EVAM) reconstruction method. This has been achieved by utilizing the multichannel EVAM constraint as a regularization term in the anisotropic denoising framework of total variation or the Mumford-Shah functional. The fundamental assumption is the weak co-primeness of blurs which guarantees the appropriate level of channel disparity and assures perfect restoration in a noise-free environment. The only input parameters, that are required, are the minimum order (size) of blurs and the noise level in the acquisition system. However, exact values of these parameters are not really needed and a rough estimate by trial and error is usually sufficient.

It was shown that the proposed algorithm gives satisfying results, compared to EVAM, even for low SNR's around 30dB. This indicates that the denoising scheme significantly stabilizes the restoration process. The channel co-primeness is a mild condition especially in real applications, since the necessary channel disparity is probably always satisfied by random processes intrinsic to a given acquisition system. For example in case of the astronomical data, atmospheric turbulence is often modeled by Gaussian masks. In theory, any two Gaussian masks have a common nontrivial factor, but the algorithm was still able to recover the image, since small fluctuations in PSF's assured the co-prime condition.

Although we have not addressed the question of computational complexity directly, we have demonstrated the ability of the algorithm to recover images of moderate size 500×500 with blurs up to 20×20.

We have not explored the influence of the blur order overestimation on image reconstruction and on convergence of the algorithm. A crucial issue for successful reconstruction, which to our knowledge has not been so far discussed in the literature, is the spatial alignment of channels. In real applications, the channel misalignment occurs very frequently and therefore channel registration must precede the MC restoration task. Clearly by shifting the mask centers, we can compensate to a certain extent for small translation misalignments. It is expected that the overestimated blur orders provide the necessary freedom which nullifies such misalignments by automatically offsetting the blurs centers during the reconstruction process. The influence of the misregistration and the role of the order overestimation are matters for debate and will be considered in our future research.

REFERENCES

[1] M. Banham and A. Katsaggelos, "Digital image restoration," *IEEE Signal Processing Magazine*, vol. 14, no. 2, pp. 24–41, Mar. 1997.

[2] D. Kundur and D. Hatzinakos, "Blind image deconvolution," *IEEE Signal Processing Magazine*, vol. 13, no. 3, pp. 43–64, May 1996.

[3] L. Rudin, S. Osher, and E. Fatemi, "Nonlinear total variation based noise removal algorithms," *Physica D*, vol. 60, pp. 259–268, 1992.

[4] C. Vogel and M. Oman, "Iterative methods for total variation denoising," *SIAM J. Sci. Comput.*, vol. 17, no. 1, pp. 227–238, Jan. 1996.

[5] ——, "Fast, robust total variation-based reconstruction of noisy, blurred images," *IEEE Trans. Image Processing*, vol. 7, no. 6, pp. 813–824, June 1998.

[6] T. Chan, G. Golub, and P. Mulet, "A nonlinear primal-dual method for total variation-based image restoration," *SIAM J. Sci. Comput.*, vol. 20, no. 6, pp. 1964–1977, July 1999.

[7] D. Geman and G. Reynolds, "Constrained restoration and the recovery of discontinuities," *IEEE Trans. Pattern Anal.*, vol. 14, no. 3, pp. 367–383, Mar. 1992.

[8] D. Mumford and J. Shah, "Optimal approximation by piecewise smooth functions and associated variational problems," *Comm. Pure Appl. Math.*, vol. 42, pp. 577–685, 1989.

[9] A. Chambolle, "Finite-differences discretizations of the mumford-shah functional," *RAIRO Math. Model. Numer. Anal.*, vol. 33, no. 2, pp. 261–288, 1999.

[10] R. Lane and R. Bates, "Automatic multichannel deconvolution," *J. Opt. Soc. Am. A*, vol. 4, no. 1, pp. 180–188, Jan. 1987.

[11] G. Ayers and J.C.Dainty, "Iterative blind deconvolution method and its application," *Optical Letters*, vol. 13, no. 7, pp. 547–549, July 1988.

[12] N. Miura and N. Baba, "Segmentation-based multiframe blind deconvolution of solar images," *J. Opt. Soc. Am. A*, vol. 12, no. 6, pp. 1858–1866, Sept. 1995.

[13] N. Miura, S. Kuwamura, N. Baba, S. Isobe, and M.Noguchi, "Parallel scheme of the iterative blind deconvolution method for stellar object reconstruction," *Applied Optics*, vol. 32, no. 32, pp. 6514–6520, Nov. 1993.

[14] R. Lane, "Blind deconvolution of speckle images," *J. Opt. Soc. Am. A*, vol. 9, no. 9, pp. 1508–1514, Sept. 1992.

[15] R. Lagendijk, J. Biemond, and D. Boekee, "Identification and restoration of noisy blurred images using the expectation-maximization algorithm," *IEEE Trans. Acoust. Speech Signal Process.*, vol. 38, no. 7, July 1990.

[16] S. Reeves and R. Mersereau, "Blur identification by the method of generalized cross-validation," *IEEE Trans. Image Processing*, vol. 1, no. 3, pp. 301–311, July 1992.

[17] A. Rajagopalan and S. Chaudhuri, "A recursive algorithm for maximum likelihood-based identification of blur from multiple observations," *IEEE Trans. Image Processing*, vol. 7, no. 7, pp. 1075–1079, July 1998.

[18] C. Ong and J. Chambers, "An enhanced NAS-RIF algorithm for blind image deconvolution," *IEEE Trans. Image Processing*, vol. 8, no. 7, pp. 988–992, July 1999.

[19] M. Ng, R. Plemmons, and S. Qiao, "Regularization of RIF blind image deconvolution," *IEEE Trans. Image Processing*, vol. 9, no. 6, pp. 1130–1138, June 2000.

[20] T. Chan and C. Wong, "Total variation blind deconvolution," *IEEE Trans. Image Processing*, vol. 7, no. 3, pp. 370–375, Mar. 1998.

[21] ——, "Convergence of the alternating minimization algorithm for blind deconvolution," *Linear Algebra Appl.*, vol. 316, no. 1-3, pp. 259–285, Sept. 2000.

[22] W. Zhu, N. Galatsanos, and A. Katsaggelos, "Regularized multichannel restoration using cross-validation," *Graphical Models and Image Processing*, vol. 57, no. 1, pp. 38–54, Jan. 1995.

[23] B. Tom, K. Lay, and A. Katsaggelos, "Multichannel image identification and restoration using the expectation-maximization algorithm," *Optical Engineering*, vol. 35, no. 1, pp. 241–254, Jan. 1996.

[24] A. Katsaggelos, K. Lay, and N. Galatsanos, "A general framework for frequency domain multi-channel signal processing," *IEEE Trans. Image Processing*, vol. 2, no. 3, pp. 417–420, July 1993.

[25] M. Kang, "Generalized multichannel image deconvolution approach and its applications," *Optical Engineering*, vol. 37, no. 11, pp. 2953–2964, Nov. 1998.

[26] G. Harikumar and Y. Bresler, "Perfect blind restoration of images blurred by multiple filters: Theory and efficient algorithms," *IEEE Trans. Image Processing*, vol. 8, no. 2, pp. 202–219, Feb. 1999.

[27] ——, "Efficient algorithms for the blind recovery of images blurred by multiple filters," in *Proceedings of ICIP 96*, vol. 3, Lausanne, Switzerland, 1996, pp. 97–100.

[28] S. Pillai and B. Liang, "Blind image deconvolution using a robust GCD approach," *IEEE Trans. Image Processing*, vol. 8, no. 2, pp. 295–301, Feb. 1999.

[29] G. Giannakis and R. Heath, "Blind identification of multichannel FIR blurs and perfect image restoration," *IEEE Trans. Image Processing*, vol. 9, no. 11, pp. 1877–1896, Nov. 2000.

[30] A. Chambolle and P. Lions, "Image recovery via total variation minimization and related problems," *Numer. Math.*, vol. 76, no. 2, pp. 167–188, Apr. 1997.

[31] R. Chan, T. Chan, and C.-K. Wong, "Cosine transform based preconditioners for total variation deblurring," *IEEE Trans. Image Processing*, vol. 8, no. 10, pp. 1472–1478, Oct. 1999.

[32] J. Kautsky, J. Flusser, B. Zitová, and S. Šimberová, "A new wavelet-based measure of image focuse," *Pattern Recognition Letters*, vol. 23, pp. 1785–1794, 2002.

[33] M. Chang, A. Tekalp, and A. Erdem, "Blur identification using the bispectrum," *IEEE Trans. Signal Processing*, vol. 39, no. 10, pp. 2323–2325, Oct. 1991.

Filip Šroubek received the B.Sc. and M.Sc. degrees in computer science from the Czech Technical University, Prague, Czech Republic in 1996 and 1998, respectively, and is currently a Ph.D. candidate in computer science at the Charles University, Prague, Czech Republic.

Since 1999, he has been with the Institute of Information Theory and Automation, Academy of Sciences of the Czech Republic, Prague. Since 2000, he has been with the Institute of Radiotechnique and Electronics, Academy of Sciences of the Czech Republic, Prague, Czech Republic.

His current research interests include all aspects of digital image processing and pattern recognition, particularly multichannel blind deconvolution, image denoising, image registration, and computer simulation and visualization of atomic collision processes.

Jan Flusser received the M.Sc. degree in mathematical engineering from the Czech Technical University, Prague, Czech Republic in 1985, the Ph.D. degree in computer science from the Czechoslovak Academy of Sciences in 1990, and the D.Sc. degree in technical cybernetics in 2001.

Since 1985, he has been with the Institute of Information Theory and Automation, Academy of Sciences of the Czech Republic, Prague. Since 1995, he has been holding the position of a head of Department of Image Processing. Since 1991, he has been also affiliated with the Charles University, Prague, and the Czech Technical University, Prague, where he gives courses on Digital Image Processing and Pattern Recognition.

His current research interests include all aspects of digital image processing and pattern recognition, namely 2-D object recognition, moment invariants, blind deconvolution, image registration and image fusion. He has authored and coauthored more than 80 research publications in these areas.

J. Flusser is a senior member of the IEEE.